Published in final edited form as:
Proc IEEE Int Symp Biomed Imaging. 2009 ; 5193092: 494–497. doi:10.1109/ISBI.2009.5193092.

3D SEGMENTATION OF THE LIVER USING FREE-FORM DEFORMATION BASED ON BOOSTING AND DEFORMATION GRADIENTS

Hong Zhang[§,†], **Lin Yang**[†,‡], **David J. Foran**[†,‡], **John L. Nosher**[‡], and **Peter J. Yim**[‡]

[§] Department of Biomedical Engineering, Rutgers University, Piscataway, NJ 08854

[†] The Center for Biomedical Imaging and Informatics, UMDNJ-RWJMS, Piscataway, NJ 08854

[‡] Department of Radiology, UMDNJ-RWJMS, Piscataway, NJ 08854

Abstract

This paper presents a novel automatic 3D hybrid segmentation approach based on free-form deformation. The algorithms incorporate boosting and deformation gradients to achieve reliable liver segmentation of Computed Tomography (CT) scans. A free-form deformable model is deformed under the forces originating from boosting and deformation gradients. The basic idea of the scheme is to combine information from intensity and shape prior knowledge to calculate desired displacements to the liver boundary on vertices of deformable surface. Boosting classifies the 3D image into a binary mask and the edgeflow generates a force field from the mask. The deformable surface deforms iteratively according to the force field. Deformation gradients cast restriction at each deformation step. The deformation converges to a stable status to achieve the final segmentation surface.

Index Terms

Liver Image Segmentation; CT; Boosting

1. INTRODUCTION

3D segmentation of the liver is critical for many clinical applications, involving volume measurement, tumor tracking and surgical planning. It plays an important role for measuring the graft volume prior to liver transplantations and it remains the focus of a large number of research projects [1]. Due to the large variation exhibited in the intensity and shape distribution of livers, the topic is still an open problem in spite of a significant amount of prior work.

Current segmentation approaches can be divided into eight categories: 1) thresholding, 2) region growing, 3) clustering, 4) Markov random field models, 5) artificial neural networks, 6) classifiers, 7) deformable models, and 8) atlas-guided approaches. Each method suffers from the challenge of large variation of livers and adjacent organs with similar CT values, especially for methods based on intensity gradients. In some cases, false boundary leakage to other organs occurs.

Coupling shape and intensity by minimizing a combination of energy [2] is a promising and robust method which recently emerged in the field. The support from the intensity can be obtained from features of voxels such as gradient, texture or probability from the statistical model. The support from shape can be obtained from Active Shape Models(ASM), Kernel PCA or sparse prior models.

There are three main issues that should be addressed in the shape-intensity segmentation framework. 1) the large variation and noise in intensities; 2) the large intra-case variation in shapes; and 3) an efficient way to combine the support from the two aspects. Several methods have resolved these issues to some degree, but most of them fail when large variations exist. Also, some approaches require explicit assumption on data distributions which place limitation on the application of these methods.

In this paper, we propose a novel segmentation algorithm which addresses these three issues. This method combines prior knowledge from intensity and shape to generate forces which are applied to a deformable model.

2. METHOD

Any given new 3D volume is encoded by an octree [3] based on entropy following pre-processing. A classification of block nodes in octree assigns the nodes into two groups: inside and outside liver. This process roughly indicates the location of liver in the 3D volume. Robust PCA is utilized to initialize the location, scale and rotation of a superquadric, which is placed on the classification result.

After initialization, the data depth of the deformation gradient to mean shape is calculated on each vertex. If the data depth is less than a threshold, the force from shape is applied. Otherwise, the force from intensity is applied. To reduce computation, the intensity support force is calculated only on mesh vertices and the force is stored at this location since it doesn't change during the whole segmentation process. The shape support force is calculated after the specific correspondence to the mean shape is determined. After the force on each vertex is calculated, the whole force field on each mesh vertex is smoothed by weighted average inside a 1-ring mesh centered at the vertex. Then a free-form deformation with 27 control points applied based on those forces. The iteration continues until a stable status is achieved. Free-form deformation is a traditional deformation tool in computer graphics which has been successfully applied to medical registration. We applied it to the medical image segmentation since it can deform freely without defining any internal force.

2.1. Preprocessing

Usually, a CT case has noise and different intra-plane and inter-plane resolutions. In order to reduce the effect of noise and anisotropy, tri-linear interpolation and anisotropic diffusion filtering [4] are applied. The resolution is 1mm at each direction after interpolation. Anisotropic diffusion filtering is

$$\frac{\partial}{\partial t} I(\bar{x}, t) = \nabla \bullet (c(\bar{x}, t) \nabla I(\bar{x}, t)), \tag{1}$$

where $I(\bar{x}, t)$ is the image, $\bar{x}$ is the voxel position and t is the iteration step. The $c(\bar{x}, t)$ is the diffusion function, and it is a monotonically decreasing function of the image gradient magnitude. A typical function is

$$c(\bar{x}, t) = \exp\left(-\left(\frac{|\nabla I(\bar{x}, t)|}{\kappa}\right)^2\right), \tag{2}$$

where $\kappa > 0$ is a constant parameter. The result after filtering is shown in Figure 1. Based on the results we can tell that the filtering step reliably suppresses noise and keeps the edges.

2.2. Intensity Force

2.2.1. Classification—Voxel intensities provide support for detecting the outer boundary of the liver. Based on its intensity, each voxel can be labeled into two groups: inside the liver and outside the liver. A classifier uses training data, i.e. labeled voxels, as prior intensity knowledge to predict the label of testing data, i.e. new voxels. Boosting is one type of classifiers that can transform a pool of weak learners into a strong learner and is widely used in segmentation, detection and tracking [5]. One of the most popular methods is the AdaBoost algorithm that generates a weak learner with different weights on training data iteratively. The weights are adjusted in each iteration and the weights of misclassified training data are increased. The new weak learner will be able to focus more on these training data. A boosting classifier [6] is applied which uses strong feature combination as input labeled training feature. The classifier contains two components. In the first part, the input is a group of training data with features and labels, and the output is a pool of weak learners with combinational feature extracted from the frequent itemset mining (FIM) algorithm. In the second part, the input is the pool of weak learners and training data, and the output is a strong learner.

2.2.2. Feature—For each voxel, a group of features are calculated as input to training or testing process. The Gabor filter has proven to be a robust texture feature extraction method [7]. In our work we use multi-scale 3D Gabor filter.

$$h(x,y,z)=\exp\left(-\left(\left(\frac{x'}{\sigma}\right)^2+\left(\frac{y'}{\sigma}\right)^2+\left(\frac{z'}{\sigma}\right)^2\right)\right) \times\exp(j2\pi(xu+yv+zw))\times\frac{1}{2\pi\sigma^3} \tag{3}$$

where

$$u=f\sin\phi\cos\theta,\ v=f\sin\phi\sin\theta,\ w=f\cos\phi. \tag{4}$$

and

$$[x'\ y'\ z']=R\times[x\ y\ z]',\sigma\in\{2,4\},\phi,\theta\in\{0,\frac{\pi}{2},\frac{2\pi}{3}\}. \tag{5}$$

The f denotes the amplitude and is set to 1 in our algorithm. The σ_x, σ_y and σ_z define the width of the Gaussian envelope in different x, y and z axis, respectively. The R defines the rotation matrix for transforming the Gaussian envelope to coincide with orientation of the sinusoid. The Gaussian scale parameters σ_x, σ_y and σ_z could be tuned to the local structures. So for each voxel, 18 (2×3×3) features are calculated. The classification result using the features above is shown in Figure 2. In the result, the majority parts of liver are accurately detected and it provides an accurate estimation of the region.

2.2.3. Refined Edgeflow—After the binary mask is generated from the classification, a refined version of the edgeflow algorithm [8] is applied to generate a force field. The vector on each voxel points to the closest boundary indicated by the previous classification. The original edgeflow is based on gradients. We extend it to 3D and simplify it without using

Gaussian convolution in order to reduce the computational time. We also modified the definition of scale of the edgeflow as the distance to its nearest boundary. At each voxel location (x, y, z) on mask M, the prediction error with scale s along $\theta(0 \le \theta \le 2\pi)$ and $\phi(0 \le \phi \le \pi)$ is

$$Error(s,\theta,\phi)=|M(x+s\sin\phi\cos\theta, y+s\sin\phi\sin\theta, z+s\cos\theta) - M(x,y,z)| \tag{6}$$

The edge likelihood is defined as:

$$P(s,\theta,\phi)=\frac{Error(s,\theta,\phi)}{Error(s,\theta,\phi)+Error(s,\theta+\pi,\pi-\phi)} \tag{7}$$

and the direction of the edgeflow is:

$$\arg\max_{\theta,\phi}\int_{\theta-\frac{\pi}{2}}^{\theta+\frac{\pi}{2}}\int_{\phi-\frac{\pi}{2}}^{\phi+\frac{\pi}{2}}P(s,\theta',\phi')d\theta' d\phi'. \tag{8}$$

Figure 3 shows an example which has been calculated in 2D to illustrate the approach. From the magnified vector field, the field demonstrates excellent convergence to boundary.

2.3. Shape Force

2.3.1. Cloud fit—The training data is a group of points which were sampled from the surfaces of the imaged livers. We use a superquadric and free-form deformation [9] to fit the data cloud and build up meshes. A superquadric is controlled by 11 parameters set T including 3 location, 3 scale, 3 rotation and 2 shape parameters. An initial superquadric is included to minimize the energy:

$$E=\sum_{i=1}^{N}[1 - F(T, x_i, y_i, z_i]^2 \tag{9}$$

where N is the number of vertices on superquadric and (x_i, y_i, z_i) is the location of i-th vertex. The F is an inside-outside function. It equals to one on the superquadric, larger than one outside and less than one inside. Twenty seven ($3 \times 3 \times 3$) control points are placed evenly. The free-form deformation is applied to minimize the sum of distances between vertices on the initial superquadric and data cloud. The result after fitting is shown in Figure 4. The cloud fits very well except for the surface patches exhibiting extremely large curvatures.

Once fitting is complete, 9 parameters including location, scale and rotation are used to align all surfaces to erase the rigid transformation. The correspondence between two surfaces is built up after realignment.

2.3.2. Deformation gradients—The active shape model (ASM) uses the co-ordinates of the data cloud points to build the shape model. The limitation of the strategy is the assumption of linear distribution of the sample points. This limitation is from principal component analysis (PCA). The proposed deformation gradients method can overcome the challenge. After finding the correspondence, a mean mesh is calculated by averaging the positions of all aligned meshes. The deformation gradients [10] is a matrix storing deformation information between two triangles $v(v_1, v_2, v_3)$ and $\hat{v}(\hat{v_1}, \hat{v_2}, \hat{v_3})$. A forth point for each triangle is calculated:

$$v_4 = v_1 + \frac{(v_2 - v_1) \times (v_3 - v_1)}{\sqrt{\left\|(v_2 - v_1) \times (v_3 - v_1)\right\|}}. \tag{10}$$

The deformation gradient J is defined as:

$$\begin{aligned} J &= \widehat{V} V^{-1} \\ V &= [v_2 - v_1, v_3 - v_1, v_4 - v_1] \\ \widehat{V} &= [\widehat{v}_2 - \widehat{v}_1, \widehat{v}_3 - \widehat{v}_1, \widehat{v}_4 - \widehat{v}_1] \end{aligned} \tag{11}$$

For each training mesh, the deformation gradients of all triangles with respect to mean mesh are calculated. All W training meshes are split into patches and all patches are assigned into N groups (W patches in each group) according to their correspondence. In each group, a distribution is built up based on data depth [11]. Each patch is a R-ring mesh around the central vertex. The R-ring mesh contains all vertices whose number of edges are in the shortest distance to central vertex is equal or less than R.

Given a new mesh, all vertices are assigned to groups according to their correspondence. The deformation gradient respect to mean mesh is calculated. If the probability of the deformation gradient is less than a threshold according to distribution, a force on the vertex is generated to increase the probability.

3. RESULTS AND DISCUSSION

The training data consisted of 10 cases of CT scans obtained from the Department of Radiology, UMDNJ with 0.7mm*0.7mm*5mm. A liver specialist in the Radiology department segmented each case slice by slice manually. The volume measurement error compared with the ground-truth annotation is 96.9%. The initial, middle and final process of the algorithm are shown in Figure 5. From the testing result we can tell that the proposed method converges to desired boundary.

In this paper, we have introduced a novel hybrid image segmentation algorithm. The intensity and shape information are combined into a unified force field which is applied on the mesh at each iteration. Based on the unified force field, free form deformation which can manage complex topology variation deforms mean shape to get a final segmentation result. There are two novelties in our methods. 1) A new shape model which can handle local affine transformation without any assumption on the variation of shapes. 2) The information from both intensity and shape are transferred into a unified force field and combined with the free form deformation.

In the future, a robust initialization and corresponding method will be developed. We will also investigate the speed up of the whole segmentation procedure, such as the parallelization of the algorithm.

References

1. Pham DL, Xu C, Prince JL. Current methods in medical image segmentation. Annual Review of Biomedical Engineering 2000;2:315–337.
2. Florin C, Paragios N, Funka-Lea G, Williams J. Liver segmentation using sparse 3d prior models with optimal data support. Information Processing in Medical Imaging 2007;4584:38–49. [PubMed: 17633687]

3. Muraki S. Volume data and wavelet transforms. IEEE Comput Graph 1993;13:50–56.
4. Bakalexis S, Boutalis Y, Mertzios B. Edge detection and image segmentation based on nonlinear anisotropic diffusion. Digital Signal Processing 2002:1203–1206.
5. Yang L, Georgescu B, Zheng Y, Meer P, Comaniciu D. 3D ultrasound tracking of the left ventricle using one-step forward prediction and data fusion of collaborative trackers. CVPR. 2008
6. Yuan J, Luo J, Wu Y. Mining compositional features for boosting. CVPR. 2008
7. Shen L, Bai L. 3D gabor wavelets for evaluating SPM normalization algorithm. Medical Image Analysis 2008;12:375–383. [PubMed: 18262824]
8. Ma WY, Manjunath S. Edgeflow: a technique for boundary detection and image segmentation. IEEE Transactions on Image Processing 2000;9:1375–1388. [PubMed: 18262975]
9. Bardinet E, Cohen LD, Ayache N. Superquadrics and free-form deformations: A global model to fit and track 3d medical data. Computer Vision, Virtual Reality and Robotics in Medicine 1995;905:319–326.
10. Sumner RW, Popovc J. Deformation transfer for triangle meshes. SIGGRAPH 2004:399–405.
11. Li J, Liu R. Data depth for nonparametric tests of multivariate locations and scales. Statistical Science 2004;19:686–696.

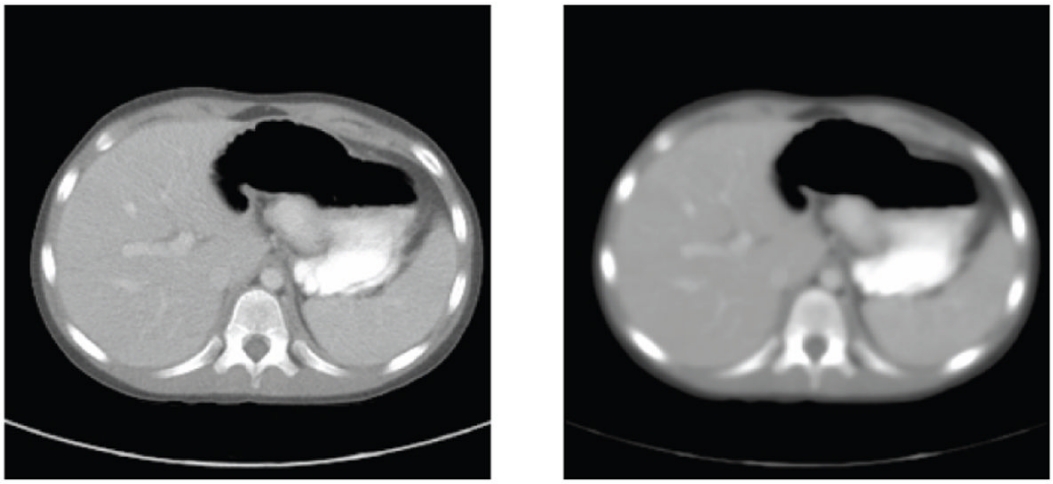

Fig. 1.
Liver CT image and filtered result

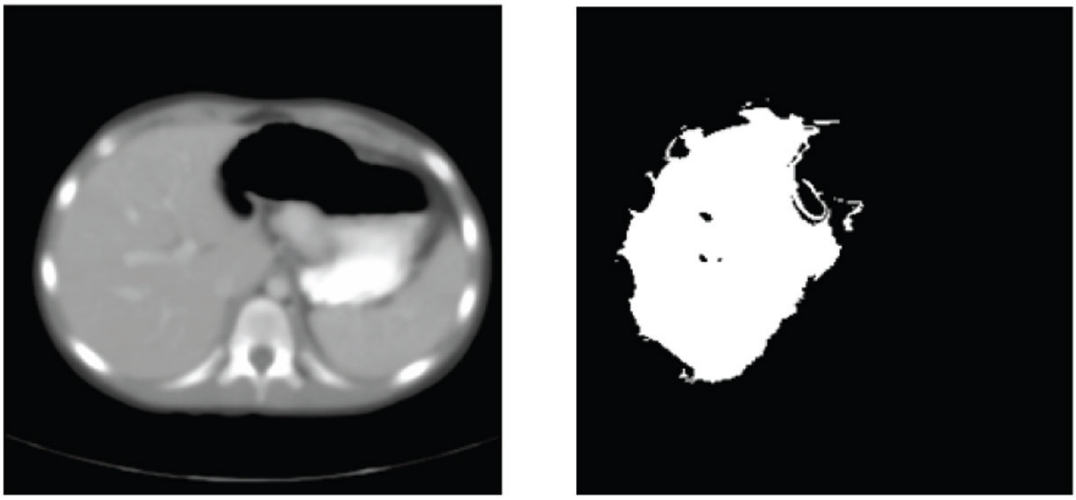

Fig. 2.
Filtered image and classification result

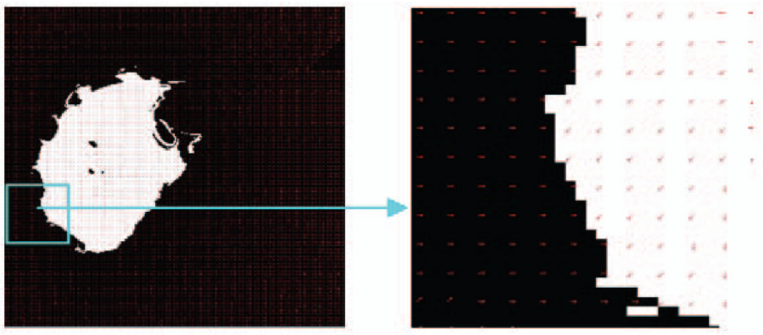

Fig. 3.
Revised edgeflow and zoom in image

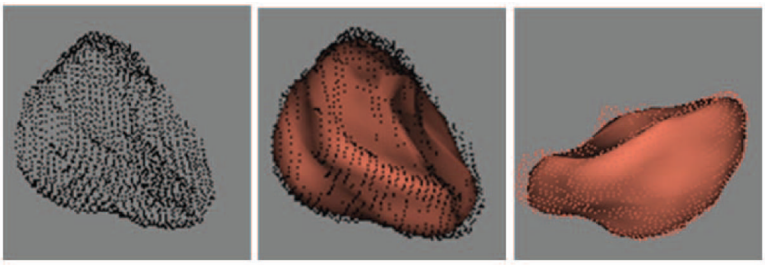

Fig. 4.
Data cloud and two fit mesh from different viewpoints

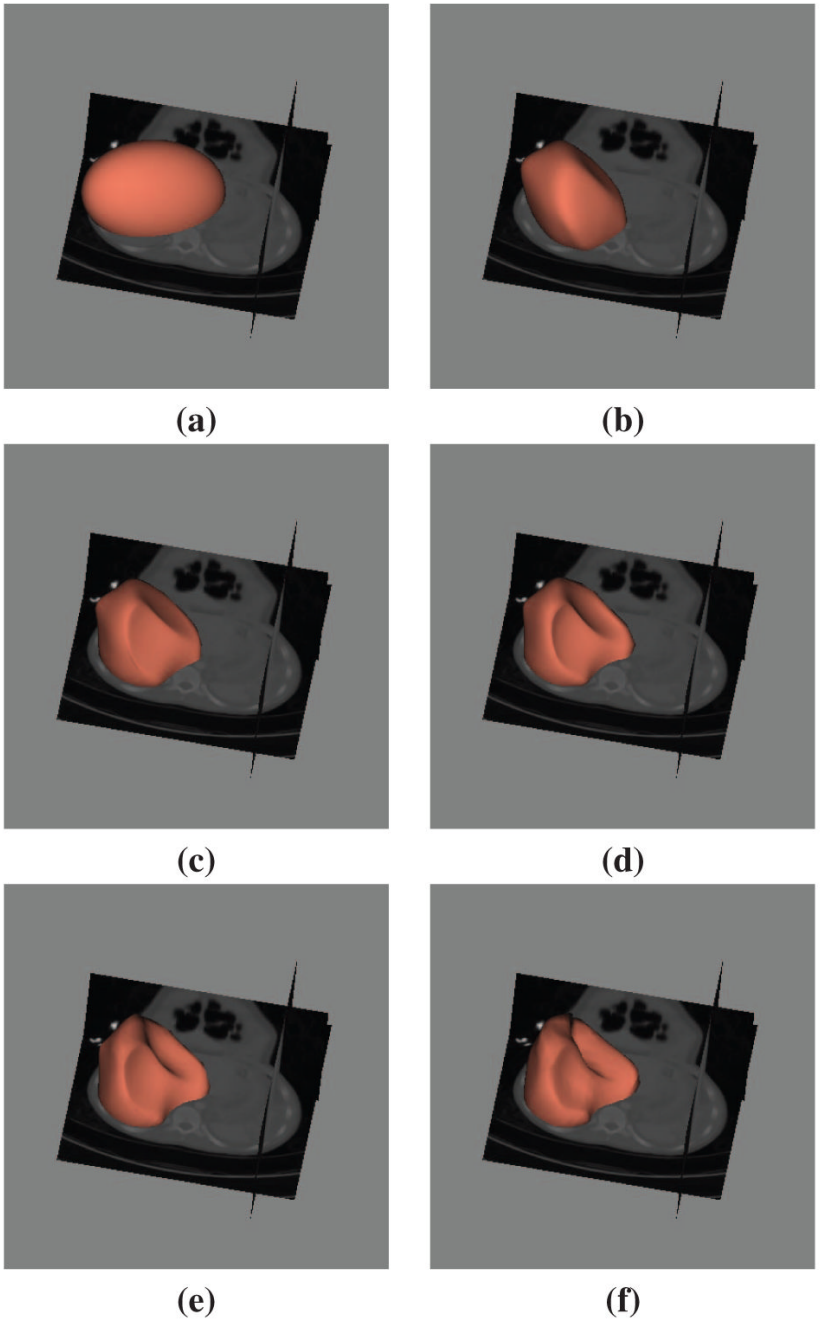

Fig. 5.
Segmentation process (a) Initial status (b)–(e) Middle status (f) Final result